Eur. Phys. J. D **11**, 59–71 (2000)

THE EUROPEAN PHYSICAL JOURNAL D

EDP Sciences

Formation of cold Cs_2 ground state molecules through photoassociation in the 1_u pure long-range state

D. Comparat, C. Drag, B. Laburthe Tolra, A. Fioretti, P. Pillet[a], A. Crubellier, O. Dulieu, and F. Masnou-Seeuws

Laboratoire Aimé Cotton[b], CNRS II, bâtiment 505, 91405 Orsay, France

Received 19 July 1999

Abstract. We report on the formation of translationally cold Cs_2 ground state molecules through photoassociation in the 1_u attractive molecular state below the $6s_{1/2}+6p_{3/2}$ dissociation limit. The cold molecules are obtained after spontaneous decay of photoassociated molecules in a MOT and in a dark SPOT. We also used polarized atoms, in the $f = 3$, $m_f = +3$ Zeeman ground state. Purely asymptotic and adiabatic calculations including hyperfine interaction and rotation are in excellent agreement with observed structures. As expected, the 1_u state is actually a pure long-range state, consisting of paired atoms, uniquely linked by the first terms of the multipole expansion of the electrostatic interaction. A temperature of 20^{+15}_{-5} μK has been measured for the molecular cloud.

PACS. 32.80.Pj Optical cooling of atoms; trapping – 33.20.-t Molecular spectra – 34.20.-b Interatomic and intermolecular potentials and forces, potential energy surfaces for collisions

1 Introduction

The experimental techniques of laser cooling of atoms in the mK–μK range and below, as well as the trapping and the manipulation of neutral atomic samples, based on radiative pressure, are now well established. Their extension to molecules is however very difficult because of the lack of two-level optical pumping schemes for population recycling [1]. Molecules have largely been unaffected by the impressive developments in laser cooling over the past decade. Exceptions are perhaps the deflection of a molecular beam [2] or the demonstration by Djeu and Whitney [3] of laser cooling by spontaneous anti-Stokes scattering, introduced long ago by Kastler as "luminorefrigeration" [4]. The latter method presents, however, poor efficiency and poor control. Laser manipulation of molecules has reached more promising development in molecular optics and interferometry [5]. Coherent population transfer between molecular states, known as STIRAP (stimulated Raman adiabatic passage) [6], offers potential devices for molecular mirrors or beam-splitters [7], which have already been developed for atoms [8–11].

An interesting specific scheme for the formation of cold molecules is to start from cold and dense atomic samples and to form cold molecules by molecular photoassociation (PA) of two cold atoms [12]. PA has been demonstrated for alkali atoms from Li to Cs [13–17], and more recently for the hydrogen atom [18]. In this process, two free cold atoms resonantly absorb one photon and produce an excited molecule in a well-defined ro-vibrational state. The excited photoassociated molecules are translationally cold (neglecting the recoil energy, they are at the same temperature as the atoms). De-excitation of the photoassociated molecules appears thus as an obvious way to form cold ground state molecules. However, photoassociation generally corresponds to a long-range excitation, so that the bound-bound spontaneous decay probability is very small [19]. Spontaneous emission leads back mostly to dissociation of the transient cold molecules into two free atoms.

In a previous letter [17], we have reported on both the first observation of molecular PA of cold cesium atoms in a vapor cell magneto-optical trap (MOT) and the first observation of translationally cold Cs_2 molecules in their triplet ground state, through PA in the 0_g^- long-range state. The efficiency of the mechanism for the formation of cold molecules comes from the existence of a Condon point at intermediate distance, corresponding to a long-range molecular well. Two different typical PA processes, either without or with formation of cold molecules are schematically shown in Figures 1 and 2, respectively. In both cases photoassociation happens at long-range distances. If spontaneous emission occurs at a short enough interatomic distance, cold ground state molecules can be formed, while spontaneous emission at a long-range distance predominantly leads to dissociation of the excited molecules. In the case of Figure 1, the vibration of the excited molecules always keeps the two atoms at a too large interatomic distance, leading generally to a negligible cold-molecule formation rate. In the case of Figure 2,

[a] e-mail: pierre.pillet@lac.u-psud.fr

[b] Laboratoire Aimé Cotton is associated with University of Paris-Sud.

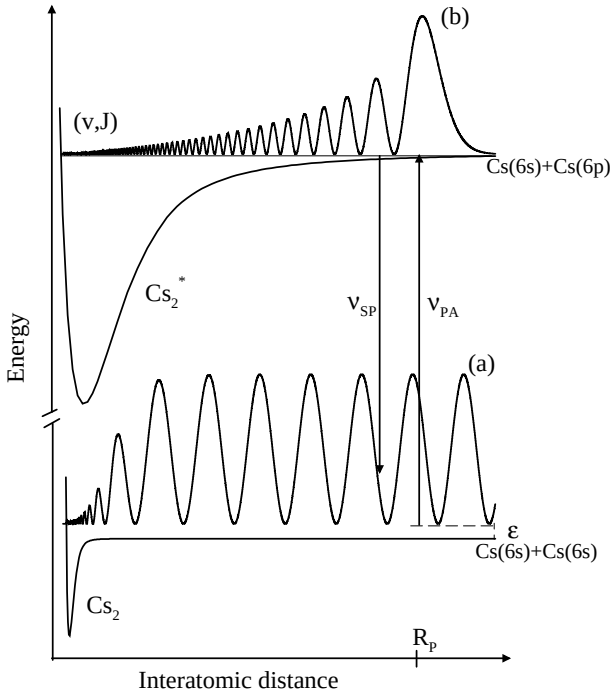

Fig. 1. Principle of molecular photoassociation of cold atoms without formation of cold molecules. The absorption and the emission of photons both occur at long-range distances (not to scale).

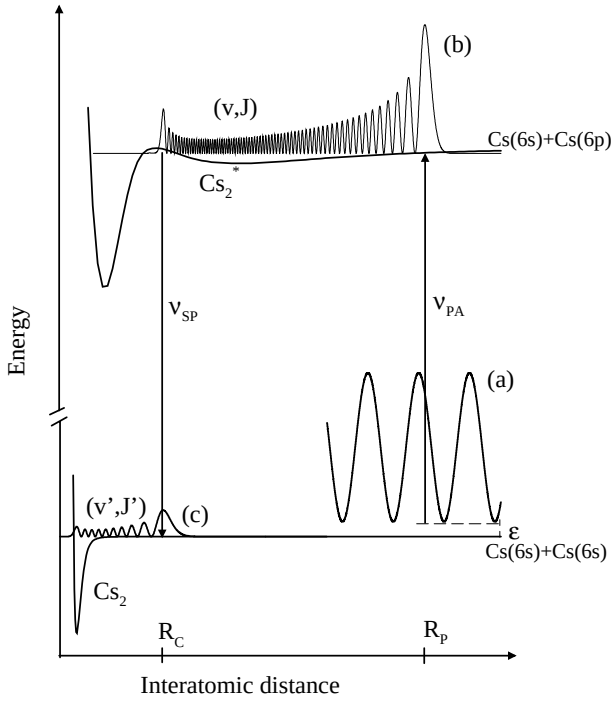

Fig. 2. Principle of molecular photoassociation of cold atoms with formation of cold molecules. The presence of an external long-range well allows the emission of photons at a Condon point at intermediate distance, leading to a bound-bound transition (not to scale).

the molecule oscillates between long-range and intermediate distances and the formation rate of stable cold molecules might be important. Four attractive long-range Hund's case (c) states can be populated by photoassociation below the $6s_{1/2} + 6p_{3/2}$ limit (see Fig. 3): 1_g, 0_u^+, 0_g^-, and 1_u (transition from the ground state to the attractive 2_u states is electric dipole forbidden). PA through 1_g and 0_u^+ states corresponds to the case of Figure 1 [20], while PA though the 0_g^- and the 1_u long-range states corresponds to the case of Figure 2. The formation of translationally cold molecules in the latter cases is due to the particular shape of the external potential wells which offers at the same time an efficient photoassociation rate and a reasonable branching ratio of spontaneous emission towards the ground state. For example, this ratio can reach up to 90% for the lowest vibrational levels of the 1_u state. More complex schemes of formation of cold molecules can be proposed, with photoassociation of highly excited molecular states [21,22]. The formation of translationally cold K_2 molecules in their singlet ground state through a photoassociation process corresponding to the case of Figure 1 has, however, been demonstrated [23]. This results from a favorable Franck-Condon factor for a particular bound-bound transition.

We have realized molecular photoassociation of cold cesium atoms in a MOT and in a dark SPOT (dark spontaneous force optical trap) [24]. In both cases we show evidence of the vibrational progression corresponding to the 1_u long-range attractive molecular state, which demonstrates the formation of cold molecules through excitation

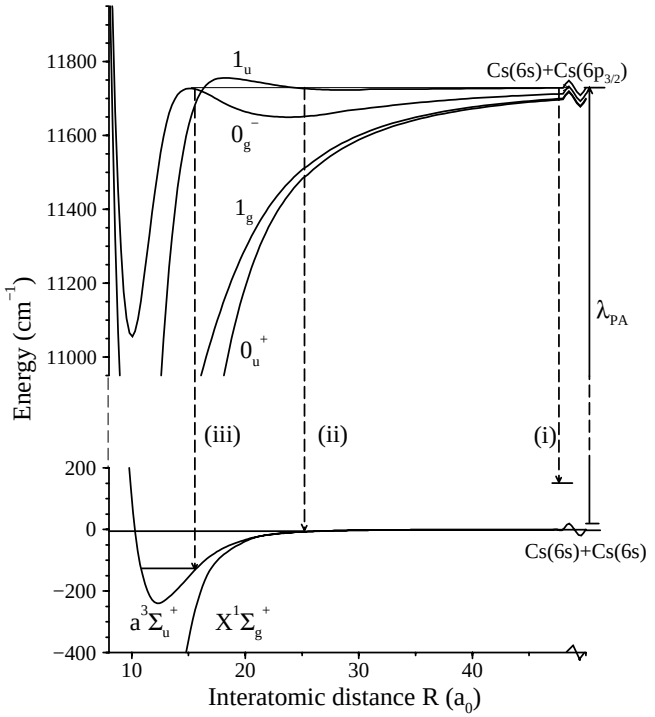

Fig. 3. Relevant potential curves of the Cs_2 molecule. Line (i) represents spontaneous emission towards continuum states, with dissociation of the molecule; lines (ii) and (iii) represent spontaneous emission towards bound states, with formation of stable cold molecules.

of the 1_u state. The pure long-range [25] 1_u state of alkali-metal dimers had only been observed for potassium [26]. In the present experiment, like in the previous ones, the PA spectrum is obtained by using photoionization detection. In both cases (MOT and dark SPOT), the vibrational levels present a large, well-resolved hyperfine and rotational structure, which is interpreted in the framework of adiabatic asymptotic calculations. We also report PA experiments with polarized atoms in the lowest energy Zeeman ground state $f = 3$, $m_f = +3$. The obtained spectra are then much more simple, and are in very good agreement with the asymptotic calculations. We have measured the temperature of the molecular cloud, which is about 20 μK starting from an atomic sample at the same temperature.

The paper is organized as follows. Section 2 is devoted to the description of the experiment. The obtained spectra of the 1_u vibrational progression are then described and analyzed taking into account the hyperfine structure and rotation (Sects. 3 and 4). In Section 5, we report experiments with polarized atoms. Finally, in Section 6, we describe the measurement of the temperature of the cold molecules and we give an estimate for the formation rate.

2 Experimental setup

The principle of the experiment is described in references [17,20,27,28]. The main difference with our previous work concerns the cold atom source which is here provided by the use of either a Cs vapor loaded MOT [29] or a dark SPOT [24]. Using a dark SPOT instead of a MOT implies a different initial state of the pair of atoms in the PA collisional process: the atoms are in the $6s_{1/2}$, $f = 3$ hyperfine level, instead of being in $f = 4$. The trapped, cold Cs atoms are illuminated with a CW-laser to produce the photoassociative transitions; one has

$$\mathrm{Cs}\,(6s_{1/2}, f = 4) + \mathrm{Cs}\,(6s_{1/2}, f = 4) + h\nu_1 \rightarrow \mathrm{Cs}_2\,(1_u(6s_{1/2} + 6p_{3/2}; v, J)) \quad (2.1)$$

for the MOT experiment, and

$$\mathrm{Cs}\,(6s_{1/2}, f = 3) + \mathrm{Cs}\,(6s_{1/2}, f = 3) + h\nu_1 \rightarrow \mathrm{Cs}_2\,(1_u(6s_{1/2} + 6p_{3/2}; v, J)) \quad (2.2)$$

for the dark SPOT experiment.

In a vapor-loaded MOT, the cold Cs atoms are produced at the intersection of three pairs of mutually orthogonal, counter-propagating $\sigma^+ - \sigma^-$ laser beams of intensity nearly 2 mW/cm^2 and of diameter 6 mm and at the zero magnetic field point of a pair of anti-Helmholtz coils with a magnetic field gradient of 15 G/cm. The residual pressure is 2×10^{-9} torr. The cooling and trapping laser beams are split from a slave diode laser (SDL 5422-H1, 150 mW, single mode, $\lambda \sim 852$ nm) injection locked to a master diode laser. The master laser (SDL 5412-H1, 100 mW) is stabilized by optical feedback from an extended, grating-ended cavity. Locking the master laser frequency to a saturated absorption line of the cesium vapor ensures its long-term stabilization. The trapping laser frequency is tuned about 13 MHz ($\simeq 2.5$ natural line-widths) to the red of the frequency $\nu_{4\rightarrow5}$ of the $6s_{1/2}, f = 4 \rightarrow 6p_{3/2}, f' = 5$ atomic transition. A repumping laser beam (SDL 5712-H1, 100 mW, $\lambda \sim 852$ nm) of frequency $\nu_{3\rightarrow4}$ resonant with the $6_{1/2}, f = 3 \rightarrow 6p_{3/2}, f' = 4$ transition is superimposed with two of the beams of the cooling laser, preventing atoms being optically pumped in the untrapped $f = 3$ hyperfine ground state. The diameter of the repumping laser is 10 mm, which is obtained by passing the collimated beam through a telescope device. In these conditions, the dimension (FWHM) of the bright cold sample ranges between 400–600 μm and the number of atoms in the trap ranges between $1 - 5 \times 10^7$, thus leading to a peak density of the order of 10^{11} atoms/cm^3. In these experimental conditions, the estimated temperature of the cold atomic sample is $T \simeq 200$ μK [30].

The MOT is shifted into a dark SPOT configuration by modifying the repumping arrangement to transfer most of the atoms ($> 90\%$) in the "dark" state $f = 3$ in the center of the trap. The repumping beam is now partly screened with a 3 mm diameter black spot of insulating tape, stuck onto a microscope slide. The spot is imaged at the center of the trapping region using a lens of focal length $l = 400$ mm, placed at a distance $2l$. Just after the lens, a beam splitter splits the repumping laser beam into two beams, which are superimposed with two cooling laser beams using polarizing beam splitters. The images of the spot for the two laser beams correspond to the center of the trapping zone. The difficulties in applying the dark SPOT technique to heavy atoms have already been discussed [31]. To obtain a large fraction of the atoms in a "dark" state, we illuminate the cold atomic sample with a laser beam of about 10 mW cm^{-2}, tuned about 25 MHz (~ 5 natural linewidths) to the blue of the frequency $\nu_{4\rightarrow3}$ of the $6s_{1/2}, f = 4 \rightarrow 6p_{3/2}, f' = 3$ atomic transition. To obtain that, the diode laser is locked on the level crossing $6s_{1/2}, f = 4 \rightarrow 6p_{3/2}, f' = 3$ and $6s_{1/2}, f = 4 \rightarrow 6p_{3/2}, f' = 5$ and the laser beam passes through an acousto-optic modulator which shifts its frequency by 200 MHz. We have verified by photoabsorption that more than 90% of the atoms in the center of the trapping zone are in the "dark" state $f = 3$ [32]. In the MOT and dark SPOT devices, atoms can be further cooled below the Doppler limit down to $T \leq 30$ μK by detuning, during 7 ms, the trapping laser to 9 natural linewidths and simultaneously reducing the beam intensities by a factor of two through a Pockels cell.

PA is achieved by continuously illuminating the cold Cs atoms with the beam of either a diode laser (SDL 5712-H1, 100 mW, $\lambda_1 \sim 852$ nm) or a Ti:sapphire laser (Coherent 899 ring laser) pumped by an argon ion laser. The maximum available power in the experiment zone is 600 mW, focused on a spot of ~ 200 μm diameter, leading to a maximum available intensity in the MOT zone of up to 1 kW cm^{-2}. However, the power of the PA laser is gradually reduced for detunings close to $\nu_{4\rightarrow5}$ in order to avoid perturbations in the MOT operation. The frequency scale is calibrated using a Fabry-Perot interferometer and the absorption lines of iodine [33]. The maximum absolute

uncertainty is estimated to be ±150 MHz, mainly due to the uncertainties on the position of the iodine lines. Thanks to the Perot-Fabry interferometer which has a free spectral range of 750 MHz, the local uncertainty is reduced to about ±10 MHz.

In general, two kinds of detection can be used to observe the photoassociation process. One can observe with a photodiode the fluorescence yield from the trap, which allows one to analyze the trap losses and to obtain vibrational progressions. However, only the 1_g, 0_u^+, and 0_g^- vibrational progressions are then clearly identified in the fluorescence spectra [20]. For the 1_u and 0_g^- vibrational progressions we used photoionization of the translationally cold Cs_2 molecules to Cs_2^+ ions, which are then detected through a time-of-flight mass spectrometer. Ionization is produced using a pulsed dye laser (dye: LDS 722; pulse duration: 7 ns; pulse energy: 1 mJ) pumped by the second harmonic of a Nd-YAG laser, running at a 10 Hz repetition rate. The dye laser is tuned to the wavelength $\lambda_2 \sim 716$ nm. Photoionization proceeds through a REMPI process (Resonance Enhanced Multi-Photon Ionization), *via* the vibrational levels of an electronic molecular state correlated to the $6s_{1/2} + 5d_{3/2,5/2}$ dissociation limit. The temporal sequence of the detection is as follows. At the trap position, a CW high-voltage field (1.7 kV) is applied by means of a pair of electric field grids spaced 15.6 mm apart. The Cs^+ and Cs_2^+ ions produced are expelled out of the interaction region to a 6 cm field-free zone which constitutes a time-of-flight mass spectrometer separating in time Cs_2^+ ions (1.9 μs delay) from Cs^+ ones (1.3 μs delay). The ions are detected by a pair of micro-channel plates and the Cs_2^+ ion signal is recorded with a gated integrator. The relative magnitude of the Cs^+ and Cs_2^+ signals depends strongly on the pulsed laser wavelength and intensity. The Cs_2^+ ion (REMPI) signal depends linearly on intensity while the Cs^+ one is quadratic, due to two-photon ionization of atomic cesium in the $6p_{3/2}, f' = 5$ excited state. The detection procedure can finally be optimized, either for 0_g^- or 1_u, by adjusting the wavelength of the pulsed laser used for photoionization. The whole acquisition is controlled by a computer running the Labtech software.

3 Experimental spectra

The Cs_2^+ ion spectrum, recorded as a function of the PA laser frequency, is shown in Figure 4. The origin of the energy scale is fixed at the $6s_{1/2}, f = 4 \rightarrow 6p_{3/2}, f' = 5$ atomic transition, which corresponds to an energy of 11 732.183 cm^{-1} [34] above the $6s_{1/2}, f = 4 + 6s_{1/2}, f = 4$ asymptote. The MOT spectrum exhibits both the 0_g^- and the 1_u vibrational progressions, while the 0_g^- progression is dominated by the 1_u one in the dark SPOT spectrum. The observed intensities corresponding to the same vibrational levels are different for the MOT and the dark SPOT experiments; the latter are on average 10 times larger. One notices also that the ground vibrational level, $v = 0$, appears in the dark SPOT spectrum but not in the MOT spectrum. Conversely, higher vibrational levels, up to $v = 12$, are observed in the MOT spectrum. The two spectra correspond to two different initial states of the collisional process (see Eqs. (2.1, 2.2)), with the two free atoms either in the $f = 4$ or the $f = 3$ state. The modulation of the line intensities, which is strikingly different in the two cases, is due to the variations of the Franck-Condon factors of the transitions between the initial state and the final ro-vibrational levels of the 1_u state. As it has already been noticed (see for instance [35]), this modulation can be used for the determination of collisional parameters such as scattering lengths; this will be reported in a forthcoming paper.

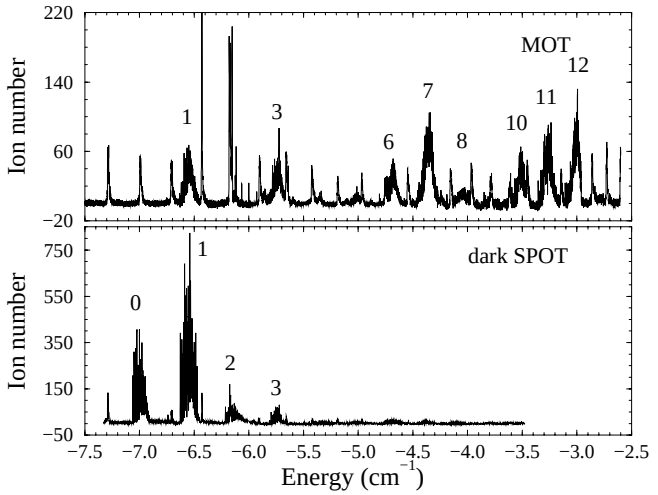

Fig. 4. Cs_2^+ ion signal *versus* frequency in the dark SPOT device (a) and in the MOT (b). The origin of the frequency scale is the dissociation limit $6s_{1/2}f = 4 + 6p_{3/2}f' = 5$.

Finally we notice that, as has previously been mentioned [17], cold molecules are produced in the MOT cold atomic sample even in the absence of the PA laser beam. The number of cold molecules produced in the same conditions in the dark SPOT is even more important. An interpretation for this production of cold molecules in the MOT has been proposed in reference [20]. Pairs of Cs atoms, separated by roughly $1500a_0$, are excited by the trapping laser to the attractive excited state and are accelerated towards each other by the attractive force until they radiatively decay. Spontaneous decay then produces pairs of atoms in the $6s_{1/2}, f = 3 + 6s_{1/2}, f = 4$ state, which can undergo photoassociation due to the trapping laser. Photoassociation and spontaneous decay finally yield cold molecules. The interpretation is even simpler for the dark SPOT: redistribution among hyperfine levels of the atomic ground sate is not necessary and photoassociation is directly obtained by the trapping laser from the $6s_{1/2}, f = 3 + 6s_{1/2}, f = 3$ two-atom state at a distance $R_0 \sim 100a_0$. In addition, the atomic density in the dark SPOT is twice as large as in the MOT.

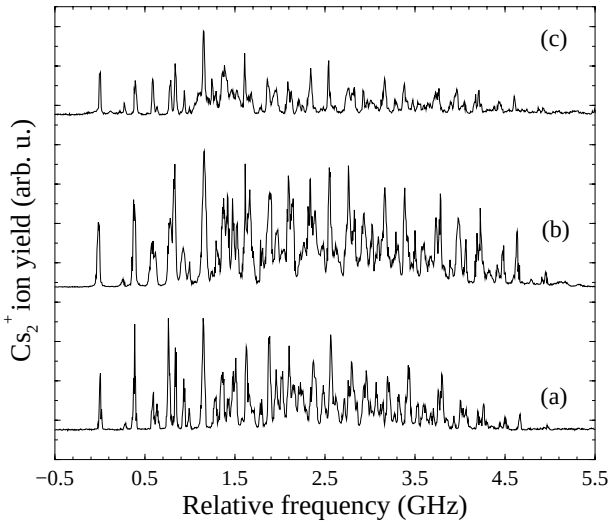

Fig. 5. Zoom of the Cs_2^+ ion signal *versus* detuning of the PA laser in the dark SPOT device, for the 1_u vibrational levels $v = 0$ (a), $v = 1$ (b), and $v = 2$ (c).

4 Hyperfine structure and rotation

Figure 5 shows the well resolved hyperfine structure of the vibrational levels $v = 0, 1$ and 2 of the 1_u state. The spectrum does not exhibit any simple structure, neither hyperfine nor rotational. We have performed systematic asymptotic calculations, including both hyperfine structure and molecular rotation, for all the electronic states involved in 1_u photoassociation. Our aim was first to interpret these complex structures. We wanted also to check whether the cold molecules produced through the 1_u series are actually "singlet" molecules, as selection rules would predict for the result of spontaneous emission starting from states with ungerade symmetry.

A precise calculation of the hyperfine structure of all adiabatic asymptotic curves for both the ground $(6s+6s)$ and the excited $(6s+6p)$ asymptotes (without rotation) was first performed by using the following procedure. We calculated the matrix elements of the relevant terms of the multipole expansion (R^{-6}, R^{-8}, and R^{-10} for $s+s$ [36], R^{-3}, R^{-6}, and R^{-8} for $s+p$ [37]) of the fine and hyperfine interactions and, for the $s+s$ asymptote, of the exchange energy (following the model of Ref. [38]). We did not introduce the exchange energy in the $s+p$ calculations because it is still small at the position of the inner wall of the 1_u potentials (about $25a_0$). For the $s+p$ asymptote, we have in fact used the C_6 and C_8 coefficients of reference [37], but instead of the value $C_3 = 10.47$ a.u. of that reference, we have put $C_3 = 10.1$ a.u., according to recent precise measurements [39]. The basis of states employed is similar to the one used by Bo Gao [40]. In our treatment, the electronic wave function is written in the rotating frame and reads

$$|(6s)\ s_1\ell_1 j_1 I\ F_1\ (6s \text{ or } 6p)\, s_2\ell_2 j_2 I\ F_2\ F_t M_F\rangle_\epsilon\,, \qquad (4.1)$$

which is an either symmetrized ($\epsilon = 1$) or antisymmetrized ($\epsilon = -1$) two-atom wave function in which the total

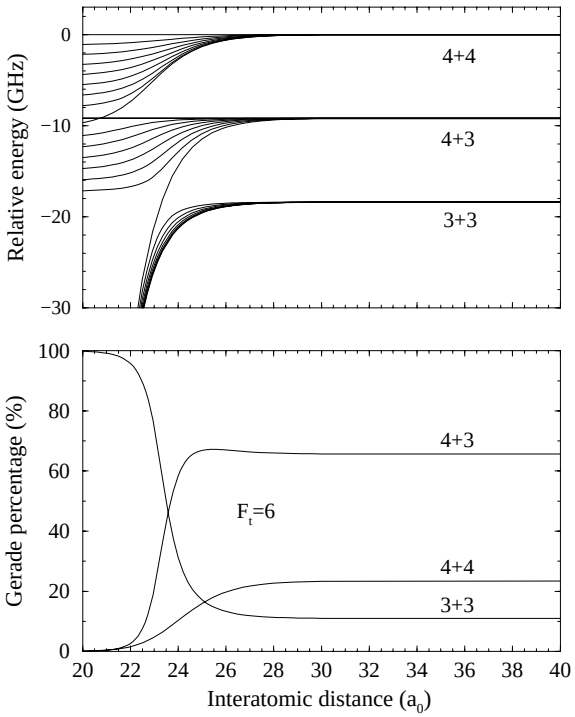

Fig. 6. Potential curves for all the $6s_{1/2} + 6s_{1/2}$ states of Cs_2 (upper graph) and percentage of gerade symmetry *vs.* interatomic distance, for the three particular states with $F_t = 6$ (lower graph). In the upper graph, as in reference [41] for Rb_2, the energy of the highest potential curve ($F_t = 8$) has been subtracted from all curves. In both graphs, the asymptotes are labeled with the values of the angular momenta F_1 and F_2 of the two atoms.

angular momentum F_1 and F_2 of the two atoms are coupled to the total F_t value, whose projection on the molecular axis is M_F; the angular momenta of the valence electron of the ith atom are noted $s_i\ell_i j_i$ and $I = 7/2$ is the nuclear spin of the cesium atom. All the relevant matrices are readily (although tediously) obtained (see Appendix): the fine and hyperfine interactions are diagonal and the dispersion terms as well as the exchange energy can be calculated through recoupling coefficients (implying $9-j$ symbols) of angular momenta (in the ground states, all dispersion terms are proportional to the unity matrix).

For the ground states, the asymptotic adiabatic potentials obtained by diagonalization of the sum of these matrices are shown in Figure 6. For the excited states, the (71 distinct[1]) adiabatic 1_u curves connected to the $s + p_{3/2}$ asymptote are shown in Figure 7.

In a large range around the bottom of the 1_u well, only $2I + 1 = 15$ different, equally spaced curves are observed (see Fig. 7). The nuclear momenta $\mathbf{I}_1$ and $\mathbf{I}_2$ of the two atoms are in this region almost completely decoupled from the electronic momenta $\mathbf{j}_1$ and $\mathbf{j}_2$. They are coupled to one another into a momentum $\mathbf{I}_t = \mathbf{I}_1 + \mathbf{I}_2$ with projection M_I on the molecule axis. The main term

[1] There are 128 different states, but the energy is the same for $+M_F$ and $-M_F$.

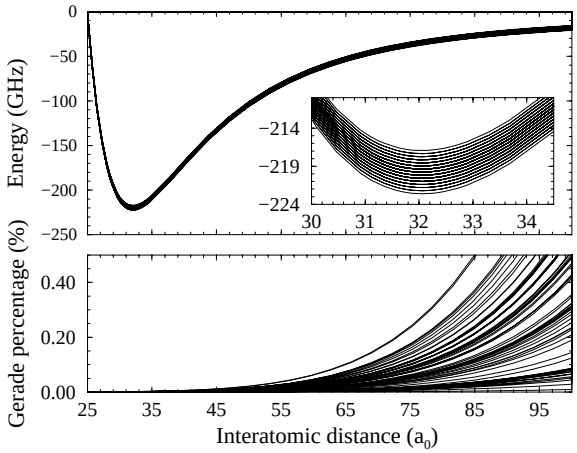

Fig. 7. Upper graph: all (71 distinct) potential curves of the 1_u state, including hyperfine structure. The inset shows a zoom of the hyperfine structure of the bottom of the well. Lower graph: percentage of gerade symmetry of these states *vs.* interatomic distance.

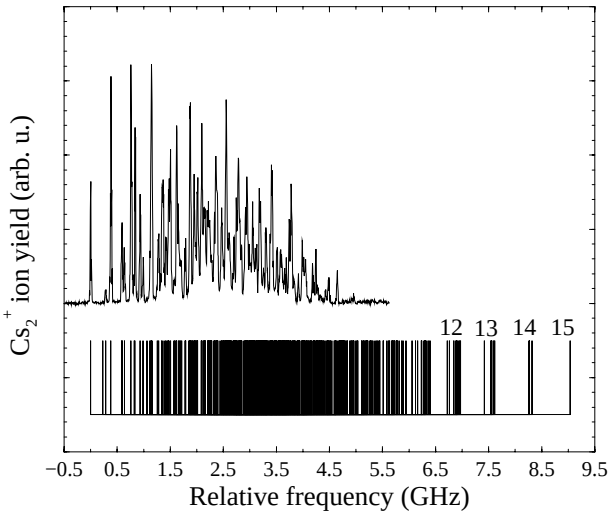

Fig. 8. Structure of the $v = 0$ line of the 1_u vibrational progression, together with the positions of all transitions, calculated as described in the text. The values of J are indicated at the red end of the structure, where it is approximately a good quantum number. The frequency of the first observable line is arbitrarily taken as zero.

of the hyperfine Hamiltonian is proportional to $\mathbf{I}_\mathrm{t} \cdot \mathbf{J}_\mathrm{t}$, where $\mathbf{J}_\mathrm{t} = \mathbf{j}_1 + \mathbf{j}_2$ is the total (spin + orbit) angular momentum of the two electrons; the energy is thus proportional to $-M_I\Omega$, where Ω is the projection of $\mathbf{J}_\mathrm{t}$ on the molecular axis. The splitting between successive hyperfine levels corresponding to a given v value of the vibrational quantum number is about 0.41 GHz while the total splitting is about 5.69 GHz, which is of the same order as the width of the observed structures.

From the result of the diagonalization, we have then calculated the gerade percentage of the adiabatic electronic states (see Appendix). In the range of interatomic distances corresponding to the observed photoassociation lines (from about $30a_0$ to $60a_0$), the symmetry of the ground state is found to be clearly dominated by the hyperfine structure: it is neither g nor u (Fig. 6)[2]; conversely the 1_u states are found purely ungerade (Fig. 7). Population of the 1_u states will thus arise from the g fraction of each initially populated $s + s$ continuum state. The same situation still holds for the gerade/ungerade symmetry in the range where cold molecules are formed (at about $30a_0$): due to the large hyperfine structure of the ground state, the cold molecules are created in mixed gerade-ungerade states, not in singlet states, as one would expect from the pure ungerade symmetry of the upper state reached after photoassociation.

As rotation and hyperfine structure seem to be quite entangled (see Fig. 5), we have made simultaneous treatment of the two effects, as in reference [26]. We have diagonalized the sum of the matrix of the asymptotic interaction, taken at a fixed interatomic distance, $R = 32a_0$, *i.e.*, at the bottom of the 1_u potential well, and of the matrix of the operator $B_v\boldsymbol{\ell}^2$, where $\boldsymbol{\ell}$ is the angular momentum of the relative nuclear motion and where B_v is the mean value of $1/(2\mu R^2)$ for the radial wave function of a given vibrational quantum number v calculated in the 1_u potential previously obtained. All these calculations are performed in a basis of states,

$$|(6s)\ s_1\ell_1 j_1 I\ F_1\ (6s \text{ or } 6p)\, s_2\ell_2 j_2 I\ F_2\ F_\mathrm{t} M_F \epsilon; FM\rangle\,, \tag{4.2}$$

which are eigenstates of the total angular momentum $\mathbf{F}$ that are obtained from the electronic states (4.1) by adding the rotational part and by symmetrizing the final wave function (see Appendix). We assume that, initially, only $(6s + 6s)\ F_1 = 3,\ F_2 = 3$ states and the first partial waves are populated [28]. Taking, then, into account the symmetry of the electronic ground states ($\epsilon = (-1)^{F_\mathrm{t}}$), the electric dipole selection rules, and the highest ℓ value, allows one to find the relevant states. For instance, for ℓ up to 3 (s, p, d, and f waves), we have to restrict ourselves to states with $\epsilon = 1$ and F varying from 0 to 9, and to states with $\epsilon = -1$ and F varying from 0 to 7. The line positions that we obtain in this way are shown in Figure 8. Remarkable agreement is obtained at the "red" end of the structure but, at the "blue" end of the structure, a number of predicted lines do not appear at all. This striking effect is due to a feature already described in reference [26], in the case of the 1_u series of $^{39}K_2$ (the resulting structure is here somewhat different because of the larger nuclear momentum of cesium). The coupling changes from the red to the blue part of the spectrum. The hyperfine structure is at first dominant and the wave functions are close to

$$\left|(6s + 6p_{3/2})\ 1u\ \Omega I_\mathrm{t} M_I \epsilon; FM\right\rangle, \tag{4.3}$$

which are symmetrized wave functions in which I_t is the total nuclear spin and M_I and Ω are respectively the

[2] The $s + s$ bound states have to be calculated in general as multichannel wave functions; channel coupling cannot of course suppress the gerade/ungerade mixing of the adiabatic potential curves.

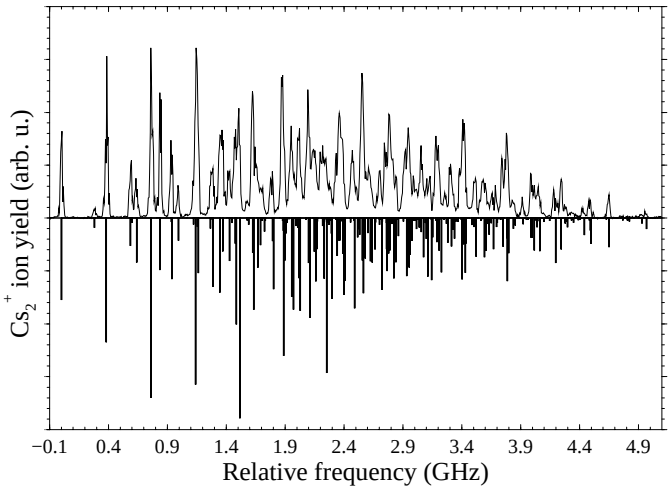

Fig. 9. Structure of the $v = 0$ line of the 1_u vibrational progression, compared in mirror with the calculated intensities. The frequency of the first observable line is arbitrarily taken as zero.

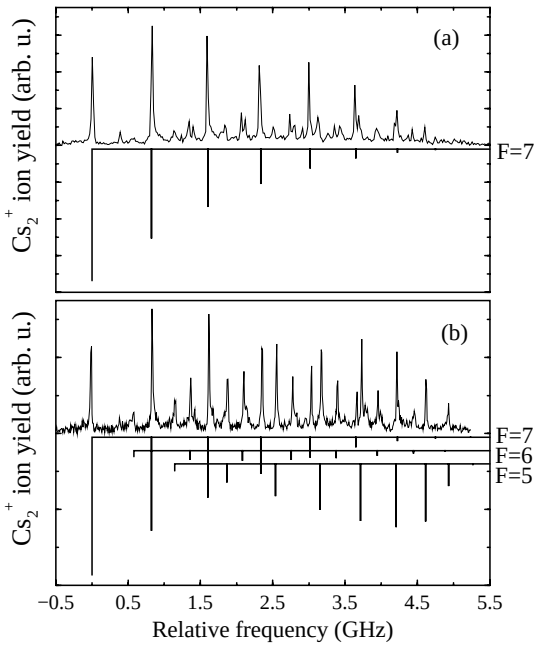

Fig. 10. Molecular PA with polarized atoms, in the Zeeman state $f = 3$, $m_f = 3$: experimental spectra (upper curves) and calculated intensities (lower curves, with different values of F displayed separately) of PA towards the $v = 1$ vibrational level of the 1_u state, in the case of σ^+ polarization (a), and linear "σ" polarization (b) of the PA laser.

projections of I_t and of the total electronic angular momentum, $J_t = 1$, on the molecular axis. At the end of the predicted structure, rotation becomes larger than hyperfine interaction and the wave functions are close to

$$\left|(6s + 6p_{3/2})\ 1u\ \Omega; JI_t\epsilon FM\right\rangle, \tag{4.4}$$

which are symmetrized wave functions in which the total electronic angular momentum is first coupled to the rotational angular momentum giving a total electronic J value, which is then coupled to the total nuclear spin I_t leading to a total value F. Only the smallest J values can be populated from initial states with small ℓ values (see Fig. 8). For instance in the case $F = 7$, $\epsilon = 1$, the last expected line corresponds to $J = 13$ and thus would require $\ell = 12$, which is assumed to be not populated. This explains why all of the blue end of the predicted structure is not observed. A complete calculation of the intensities (see Appendix), in which the only adjustable parameters are the initial populations of the different partial waves (from s to g, here), confirms this result. No breakdown of the adiabatic approximation appears and the calculations agree very well with experiment (see Fig. 9).

5 Molecular photoassociation with polarized cold atoms

We have also prepared polarized atoms in the lowest energy ground state Zeeman sub-level $f = 3$, $m_f = +3$. The polarization procedure is given by the following temporal sequence. First, at the time $t = 0$, we switch off the MOT cooling laser and the magnetic field gradient for 8 ms and 4 ms, respectively, and simultaneously we apply a 4 G magnetic field oriented along the PA laser propagation direction. At $t = 1$ ms, corresponding to the rise time of the magnetic field, we apply a pulsed polarization laser (pulse duration 3 ms; pulse intensity $\sim 20\ \mu W/cm^2$) propagating along the same axis as the PA laser with a σ^+ polarization, and tuned to the $6s_{1/2}, f = 4 \rightarrow 6p_{3/2}, f' = 4$ atomic transition. At this moment the cold atoms are in the Zeeman sublevel $f = 4$, $m_f = +4$. After an additional delay of 500 μs ($t = 1.5$ ms) we switch off the MOT repumping laser. As the direction of propagation of the polarization laser makes a small angle (about 3°) with the magnetic field, the polarization laser contains some π polarization which allows the optical pumping from the $f = 4$, $m_f = +4$ Zeeman sublevel to $f = 3$, $m_f = +3$ (with the notation of the Appendix, $F_t = 6$, $M''_F = 6$). Simultaneously ($t = 1.5$ ms), we apply the PA laser during a time of 2.5 ms. We then detect the formation of cold molecules at the end of the PA laser pulse. The laser pulses are obtained by using acousto-optic modulators or Pockels cells and the magnetic field is switched on and off by using a transistor. The measured atomic polarization is larger than 85%. In this experiment the temperature was low enough to permit consideration of only s and p partial waves and, in addition for polarized atoms, the symmetry of the wave function prohibits odd values of ℓ. As a consequence, the s-wave provided the main contribution to the line intensities, which has been checked on the 0_g^- spectrum.

Figure 10 shows the well resolved hyperfine structure of the vibrational level $v = 1$ of the 1_u state in the case of a PA laser with a polarization σ^+ (a) and linear (noted "σ" hereafter) (b). The experimental spectra are much simpler than those obtained with unpolarized atoms.

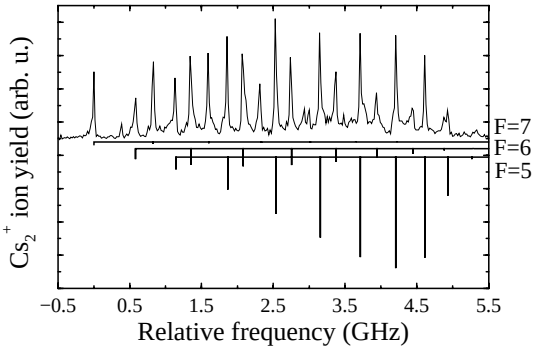

Fig. 11. Molecular PA with polarized atoms: experimental spectrum (upper curve) and calculated intensities (lower curve, with different values of F displayed separately) of PA towards the $v = 1$ vibrational level of the 1_u state, in the case of σ^- polarization of the PA laser.

For spectrum (a), we can only excite states with $M = 7$, $F = 7$. For spectrum (b), one has $M = 5$ and 7, and thus $F = 7$, 6, and 5. The calculations show good agreement with the experimental spectra, the small discrepancies probably coming from the imperfections of the atomic and laser polarizations. Figure 11 shows the spectrum obtained with a σ^- polarization of the PA laser. One would expect $M = 5$, and thus $F = 5$, 6, and 7. The calculation predicts very small intensities for the $F = 7$ lines (see Fig. 11), while the observed intensities of the $F = 7$ lines are of the same order as for the "σ" PA laser spectrum. This striking discrepancy between experiment and theory is probably due to an imperfect σ^- polarization. Because of the huge ratio of 91 between the squares of the two 3-j coefficients (see Eq. (A.2) in the Appendix),

$$\begin{pmatrix} F & 1 & F'_{\rm t} \\ -M''_F - p & p & M''_F \end{pmatrix}^2 = \begin{pmatrix} 7 & 1 & 6 \\ -7 & 1 & 6 \end{pmatrix}^2 = \frac{1}{15}\,,$$

$$\begin{pmatrix} 7 & 1 & 6 \\ -5 & -1 & 6 \end{pmatrix}^2 = \frac{1}{1365}\,,$$

which are involved in the σ^+ and σ^- calculation, respectively, a very small fraction of σ^+ polarization can change drastically the spectrum. An error of one degree in the orientation of the quarter-wave plate is enough to explain the observed result.

6 Molecular temperature and formation rate

In previous papers [17,20], we have shown how the spatial analysis of the ballistic expansion of the falling molecular cloud yields a measure of the temperature of the molecular cloud. The ground-state cold Cs_2 molecules are photoionized to Cs_2^+ ions, using here the dye laser focused on a spot of 300 μm diameter. In the case of cold molecules formed through photoassociation in the 0_g^- state, temperatures of about 300 μK and 85 μK have been measured

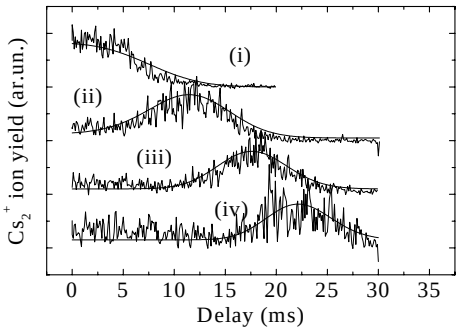

Fig. 12. Temperature measurement through time of flight: recordings (i–iv) correspond to the temporal analysis of the Cs_2^+ ion signal at the MOT position (i) and at 0.95 mm (ii), 1.90 mm (iii) and 2.85 mm (iv) below the MOT position.

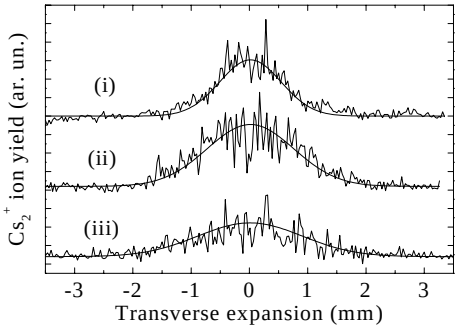

Fig. 13. Temperature measurement through ballistic expansion: recordings (i–iii) correspond to the spatial analysis of the Cs_2^+ ion signal at the MOT position (i) and 1.90 mm (ii) and 3.80 mm (iii) below the MOT position.

for operating conditions, corresponding to atomic temperatures of respectively 200 μK and 30 μK; the molecular temperature appears to be slightly higher than that of the trapped atomic sample. This discrepancy is due to the difficulty of performing a precise determination of the falling height. To improve accuracy, we have done two kinds of measurements of the molecular temperature, for both 0_g^- and 1_u photoassociation. The first one involves photoassociating the cold atomic sample during a time of 3 ms. The fall of the molecular cloud is then temporally analyzed at different distances below the atomic trap, as shown in Figure 12. The theoretical fit of the experimental data gives access not only to the determination of the temperature, but also to the height of the fall. The analysis of the ballistic expansion for different heights allows one to verify the measurements of the temperature. Figure 13 depicts the spatial analysis of the falling molecular cloud, which yields a measure of the temperature of the molecules. A model based on reference [42], taking into account the formation and the fall of the cold molecules, allows one to derive the molecular temperature from the data [43]. A temperature as low as 20^{+15}_{-5} μK was found in our experiment. The atomic temperature was measured similarly by photoionizing the cold Cs atoms into Cs^+ ions. The measured

atomic temperature lies in the range 20–30 μK, with no difference between molecular and atomic temperatures.

From the number of Cs_2^+ ions detected at a detuning corresponding to a given ro-vibrational level of the 1_u state, it is possible to estimate the corresponding number of cold molecules $N_{\rm cold}$ produced in the trap. The number $N_{\rm ions}$ of Cs_2^+ ions detected in the experiments is indeed proportional to the number of cold molecules; one can write

$$N_{\rm ions} = \eta_{\rm ion} N_{\rm cold},$$

where $\eta_{\rm ion}$ includes the microchannel plate efficiency, which is about 35%, the ion recollection rate, which is about 80%, and the efficiency of the ionization process, including both the excitation towards the intermediate step (levels of the $(2)^3\Pi_g(6s+5d)$ excited molecular states serve as intermediate step) and the ionization itself. The efficiency of the latter process is estimated to lie between 10 and 40%. We obtain for the $\eta_{\rm ion}$ parameter a value between 0.03 and 0.1. Typically up to 500 ions are detected per shot, which corresponds to 5 000–15 000 cold molecules in the trap zone. The cold molecules stay in the trap zone for a characteristic time of 10 ms. One can thus infer a rate of cold-molecule formation of about one million per second.

7 Conclusion

In conclusion, we have reported PA spectroscopy of Cs_2 for the long-range 1_u state below the $6s_{1/2} + 6p_{3/2}$ dissociation limit. Like the long-range 0_g^- state, the 1_u potential provides a Condon point at intermediate distance as a result of its double-well shape. The existence of this Condon point creates an efficient channel for the creation of ground state molecules (neither singlet nor triplet, because of the mixing due to hyperfine structure) through spontaneous emission. In the case of the 1_u state, the outer well is long-range enough to permit the total neglect of the molecular exchange terms of the interaction. The cohesion of the molecular system is given here by electrostatic multipole interaction between the two atoms. This system appears as paired atoms exchanging their excitation by multipole interaction. For the other alkalis, the 1_u outer well does not offer such a channel for the formation of cold molecules; the situation seems more favorable to the formation of cold molecules for rubidium, which should present a Condon point at intermediate distance for the 0_g^- state. The use of polarized atoms offers new possibilities for PA experiments, in particular for the determination of scattering lengths or Feshbach resonances, which will be very helpful in the future development of Bose-Einstein condensation of cesium.

PA of cold atoms for formation of stable cold molecules opens a very promising novel field of investigation. Several difficulties remain to be resolved. The formed molecules are indeed cold both translationally and rotationally [28], but to get them vibrationally cold is an interesting challenge, the cold molecular sample being in a statistical mixture of different vibrational states. Stimulated Raman photoassociation, where the emission on a given bound-bound transition is stimulated, is probably a good way to obtain all the cold molecules in a well-defined ro-vibrational level. Further Raman transitions will allow them to be brought to the lowest energy level, $v = 0$, $J = 0$. In order to develop applications using cold molecules, it will be necessary to be able to store them. Dipolar or magnetic traps should be realizable for this purpose [45–47]. The trapping of translationally cold Cs_2 molecules has already been performed with the use of a CO_2 laser [47]. Starting from colder and denser atomic samples, colder and denser molecular clouds will certainly be obtained in the near future and this could be a way towards Bose-Einstein condensation of molecules.

We gratefully thank C. Amiot and C. Williams for many valuable discussions about theory and S. Guibal and L. Pruvost for helpful advices about the experiment. We are also indebted to I. Mourachko in the development of the dark SPOT device. A. Fioretti was recipient of an European grant, TMR program, contract number ERBFMBICT961218; his present address is Instituto Nationale di Fisica della Materia, Dipartimento di Fisica, Piazza Torricelli 7, 50127 Pisa, Italy.

Appendix A: Asymptotic calculations in a hyperfine coupled two-atom state basis

A.1 Electronic states

All our calculations use a basis of electronic states defined in the molecular frame whose z-axis is the internuclear axis:

$$|s_1 l_1 j_1\, I\, F_1\; s_2 l_2 j_2\, I\, F_2 F_{\rm t} M_F\rangle_\epsilon\,;$$

the angular momenta of the two electrons are noted $s_i l_i j_i$ ($i = 1, 2$), I is the nuclear spin and the total angular momenta F_1 and F_2 of the two atoms are coupled to a value $F_{\rm t}$, with projection on the molecule axis M_F; the wave function is antisymmetrical with respect to the exchange of electronic coordinates ($1 \longleftrightarrow 2$) and either symmetrical ($\epsilon = 1$) or antisymmetrical ($\epsilon = -1$) with respect to simultaneous exchange of electronic and nuclear coordinates and spins ($\{1, A\} \longleftrightarrow \{2, B\}$). Such a basis is especially convenient for dealing with the hyperfine structure, which is then diagonal and which can be expressed using experimental atomic splittings. Of course, the successive terms of the multipole expansion are somewhat more difficult to obtain than in the usual basis, where nuclear spin momenta are assumed to be decoupled from the other angular momenta; however the calculation requires only angular momentum recoupling and is tedious but simple. For valence electrons with different

$$|s\ell_1 j_1\, I\, F_1\ s\ell_2 j_2\, I\, F_2\ F_{\rm t} M_F\rangle_\epsilon = \sum_{\substack{J_{\rm t},I_{\rm t},S_{\rm t},L_{\rm t},\\ M_J,M_I,M_S,M_L,\\ m_1,m_2}} \widehat{F}_1\widehat{F}_2\widehat{j}_1\widehat{j}_2\widehat{J}_{\rm t}\widehat{I}_{\rm t}\widehat{S}_{\rm t}\widehat{L}_{\rm t}$$
$$\times(J_{\rm t}M_J I_{\rm t}M_I \mid F_{\rm t}M_F)(S_{\rm t}M_S L_{\rm t}M_L \mid J_{\rm t}M_J)(\ell_1 m_1 \ell_2 m_2 \mid L_{\rm t}M_L) \left\{ \begin{array}{ccc} s & \ell_1 & j_1 \\ s & \ell_2 & j_2 \\ S_{\rm t} & L_{\rm t} & J_{\rm t} \end{array} \right\} \left\{ \begin{array}{ccc} j_1 & I & F_1 \\ j_2 & I & F_2 \\ J_{\rm t} & I_{\rm t} & F_{\rm t} \end{array} \right\} |I_{\rm t}M_I\rangle_{A,B}\, |S_{\rm t}M_S\rangle^{1,2}$$
$$\times\frac{1}{2}(|\ell_1 m_1\rangle_A^1\, |\ell_2 m_2\rangle_B^2 - (-1)^{2s-S_{\rm t}}\, |\ell_1 m_1\rangle_A^2\, |\ell_2 m_2\rangle_B^1 - \epsilon(-1)^{2I-I_{\rm t}}\, |\ell_1 m_1\rangle_B^1\, |\ell_2 m_2\rangle_A^2 + \epsilon(-1)^{2s-S_{\rm t}+2I-I_{\rm t}}\, |\ell_1 m_1\rangle_B^2\, |\ell_2 m_2\rangle_A^1), \quad \text{(A.1)}$$

$$|(s+s)\ I\, F_1\ I\, F_2\ F_{\rm t} M_F\rangle_\epsilon = \sum_{I_{\rm t},S_{\rm t},M_I,M_S} \frac{1-\epsilon(-1)^{S_{\rm t}+2I+I_{\rm t}}}{2} \widehat{F}_1\widehat{F}_2\widehat{I}_{\rm t}\widehat{S}_{\rm t}(S_{\rm t}M_S I_{\rm t}M_I \mid F_{\rm t}M_F) \left\{ \begin{array}{ccc} 1/2 & I & F_1 \\ 1/2 & I & F_2 \\ S_{\rm t} & I_{\rm t} & F_{\rm t} \end{array} \right\}$$
$$\times\ \frac{1}{\sqrt{2}}\, |I_{\rm t}M_I\rangle_{A,B}\, |S_{\rm t}M_S\rangle^{1,2}\ \left(|00\rangle_A^1\, |00\rangle_B^2 + (-1)^{S_{\rm t}}\, |00\rangle_A^2\, |00\rangle_B^1\right) \quad \text{(A.2)}$$

quantum numbers (like in the $s+p$ configuration), one has

see equation (A.1) above

where the notation $\widehat{J}$ means $\sqrt{2J+1}$, the large brackets are nine-j symbols and the $(j_1 m_1 j_2 m_2 \mid j_3 m_3)$ are Clebsch-Gordan coefficients. For electrons with the same quantum numbers, like in the $s+s$ configuration, it simplifies to

see equation (A.2) above.

Fine and hyperfine interactions are diagonal in this basis. The matrix elements are simple functions of F_1, F_2, and F_t related to the experimental values of the atomic fine and hyperfine splittings given in Table 1.

The matrix elements of the operators which represent the first terms of the dipole expansion have been obtained using the results of references [36,37]. For the $s+s$ asymptote, all the corresponding matrices are proportional to unit matrices and, for the $s+p$ asymptote, one has simply to notice, by comparing the electronic spin and orbital parts of the expansion with the well-known Hund's case (a) wave functions, that the parameter p of reference [37] is equal to $\eta = \epsilon(-1)^{2I+I_{\rm t}}$ and that the parameter σ is $(-1)^{S_{\rm t}}$. For both asymptotes, the matrix elements of the exchange energy depend only on $S_{\rm t}$. All matrix elements are thus readily calculated from equations (A.2, A.1). The asymptotic interaction is diagonal by blocks with given M_F and ϵ values. In the $s+s$ case, it can be proven in addition that $F_{\rm t}$ is a good quantum number and that the matrix elements do not depend on M_F.

Diagonalization of the entire interaction matrix in the relevant range of interatomic distance yields the asymptotic part of all adiabatic potential curves including hyperfine structure; there are 30 (resp. 854) different curves for the $s+s$ (resp. $s+p$) asymptote. The gerade or ungerade type of the decoupled wave functions of the right-hand members (which are molecular functions in Hund's (a) case) is given by the sign of η: it is gerade (resp. ungerade) if η is equal to 1 (resp. -1). From the eigenvectors, one thus directly obtains, using again equations (A.2, A.1), the gerade/ungerade percentages of each potential curve as a function of the interatomic distance.

Table 1. Hyperfine splittings of the lowest levels of atomic cesium. The fine structure splitting between the centers of gravity of levels $6p_{1/2}$ and $6p_{3/2}$ is equal to 554.11 cm^{-1}.

levels	ΔE (GHz)
$6s_{1/2}\ F=3 \rightarrow 6s_{1/2}\ F=4$	9.192
$6p_{1/2}\ F=3 \rightarrow 6p_{1/2}\ F=4$	1.1676
$6p_{3/2}\ F=2 \rightarrow 6p_{3/2}\ F=3$	0.151
$6p_{3/2}\ F=3 \rightarrow 6p_{3/2}\ F=4$	0.201
$6p_{3/2}\ F=4 \rightarrow 6p_{3/2}\ F=5$	0.251

A.2 Rotation and symmetrization

To introduce the rotational effects, one has first to construct wave functions including the relative motion of the two nuclei. Such wave functions can be written either in the molecular frame (non-symmetrized "molecular" basis)

$$|sl_1 j_1\, I\, F_1\ sl_2 j_2\, I\, F_2 F_t M_F\, \epsilon; FM\rangle_{\rm mol,ns}$$
$$\equiv |\gamma F_{\rm t} M_F\, \epsilon; FM\rangle_{\rm mol,ns}$$
$$= |sl_1 j_1\, I\, F_1\ sl_2 j_2\, I\, F_2 F_{\rm t} M_F\rangle_\epsilon\, R^F_{M_F M}(\theta,\varphi), \quad \text{(A.3)}$$

where the angular wave function, $R^F_{M_F M}(\theta,\varphi)$, is simultaneously an eigenfunction of $\mathbf{F}^2$ and of its projections on the fixed axis (M) and on the rotating axis (M_F),

$$ {}_{\rm mol}\langle \gamma F_{\rm t}\, M_F\, \epsilon; FM|\, H_{\rm asympt}\, \big|\overline{\gamma}\overline{F}_{\rm t}\, M_F\, \epsilon; FM\big\rangle_{\rm mol} = {}_{\epsilon}\langle sl_1j_1\, I\, F_1\ sl_2j_2\, I\, F_2F_{\rm t}M_F|\, H_{\rm asympt}\, \big|sl_1\overline{j}_1\, I\, \overline{F}_1\ sl_2\overline{j}_2\, I\, \overline{F}_2\overline{F}_{\rm t}M_F\big\rangle_{\epsilon}\,, \quad \text{(A.11)} $$

or in the fixed frame (non-symmetrized "atomic" basis)

$$ \begin{aligned} |sl_1j_1\, I\, F_1\ sl_2j_2\, I\, F_2F_{\rm t}\, \epsilon; \ell FM\rangle_{\rm at,ns} &\equiv |\gamma F_{\rm t}\, \epsilon; \ell FM\rangle_{\rm at,ns} \\ &= \textstyle\sum_{M''_F,M_F,m}(F_{\rm t}M_F\ell m \mid FM) \\ &\times D^F_{M''_FM_F}(\omega)\, |sl_1j_1\, I\, F_1\ sl_2j_2\, I\, F_2F_{\rm t}M''_F\rangle_{\epsilon}\ Y_{\ell m}(\theta,\varphi). \end{aligned} \quad \text{(A.4)} $$

As the two cesium atoms are bosons, the wave function must be fully symmetrical. For the atomic basis, one has simply to use states (A.4) with $\epsilon = (-1)^{\ell}$; we write

$$ |\gamma F_{\rm t}\ell\,; FM\rangle_{\rm at} = \big|\gamma F_{\rm t}\, \epsilon = (-1)^{\ell}\ell; FM\big\rangle_{\rm at,ns}\,. \quad \text{(A.5)} $$

In the molecular basis, the symmetrization gives

$$ \begin{aligned} |\gamma F_{\rm t}\, M_F\, \epsilon; FM\rangle_{\rm mol} = \frac{1}{\sqrt{2}}\{&|\gamma F_{\rm t}M_F\, \epsilon; FM\rangle_{\rm mol,ns} \\ &+ \epsilon(-1)^{F_{\rm t}+F}|\gamma F_{\rm t}\, -M_F\, \epsilon; FM\rangle_{\rm mol,ns}\} \end{aligned} \quad \text{(A.6)} $$

if $M_F \geq 0$ and

$$ |\gamma F_{\rm t}0\, \epsilon; FM\rangle_{\rm mol} = \big|\gamma F_{\rm t}0\, \epsilon = (-1)^{F_{\rm t}+F}; FM\big\rangle_{\rm mol,ns} \quad \text{(A.7)} $$

if $M_F = 0$. The transformation from the atomic to the molecular basis is given (for $M_F \geq 0$ and $\epsilon = (-1)^{F_{\rm t}+F}$ if $M_F = 0$), by

$$ \begin{aligned} |\gamma F_{\rm t}\, M_F\, \epsilon; FM\rangle_{\rm mol} = &\sum_{\ell(\epsilon=(-1)^{\ell})} w(F_{\rm t},\ell,F,M_F) \\ &\times |\gamma F_{\rm t}\ell; FM\rangle_{\rm at} \end{aligned} \quad \text{(A.8)} $$

and, reciprocally, from the molecular to the atomic basis, by

$$ \begin{aligned} |\gamma F_{\rm t}\,\ell\,; FM\rangle_{\rm at} = &\sum_{M_F\geq 0} w(F_{\rm t},\ell\,,F,M_F) \\ &\times |\gamma F_{\rm t}\, M_F\, \epsilon; FM\rangle_{\rm mol}\,, \end{aligned} \quad \text{(A.9)} $$

with $\epsilon = (-1)^{\ell}$ if $M_F > 0$ and $\epsilon = (-1)^{F_{\rm t}+F}$ if $M_F = 0$; the w coefficient is equal to

$$ w(F_{\rm t},\ell\,,F,M_F) = \sqrt{(2-\delta_{M_F,0})}\frac{\widehat{\ell}}{\widehat{F}}(F_{\rm t}M_F\ell 0 \mid FM_F). \quad \text{(A.10)} $$

The matrix elements of the asymptotic interaction $H_{\rm asympt}$ (fine and hyperfine structures, first terms of the dipole expansion and exchange energy) in the molecular basis are diagonal in M_F, ϵ, F, and M,

see equation (A.11) above

with, for $M_F = 0$, $\epsilon = (-1)^{F_{\rm t}+F} = (-1)^{\overline{F}_{\rm t}+F}$ ($F_{\rm t}$ and $\overline{F}_{\rm t}$ must be of the same parity). The matrix elements of the operator $\boldsymbol{\ell}^2 = (\mathbf{F}-\mathbf{F}_{\rm t})^2$ are easily computed in the molecular basis; they are diagonal in γ, $F_{\rm t}$, ϵ, and F and one has

$$ \begin{aligned} &{}_{\rm mol}\langle \gamma F_{\rm t}\, M_F\, \epsilon; FM|\, \boldsymbol{\ell}^2\, \big|\gamma F_{\rm t}\, \overline{M}_F\, \epsilon; FM\big\rangle_{\rm mol} = \\ &\qquad \sum_{\ell(\epsilon=(-1)^{\ell})} w(F_{\rm t},\ell\,,F,M_F)w(F_{\rm t},\ell\,,F,\overline{M}_F), \end{aligned} \quad \text{(A.12)} $$

with the selection rule $M_F - \overline{M}_F = 0, \pm 1$. For the diagonal matrix elements, the sum takes the simple form

$$ \begin{aligned} &{}_{\rm mol}\langle \gamma F_{\rm t}\, M_F\, \epsilon; FM|\, \boldsymbol{\ell}^2\, |\gamma F_{\rm t}\, M_F\, \epsilon; FM\rangle_{\rm mol} = \\ &\qquad \hbar^2(F_{\rm t}(F_{\rm t}+1) + F(F+1) - 2(M_F)^2). \end{aligned} \quad \text{(A.13)} $$

In order to compute systematically the intensities of the 1_u photoassociation lines, we define a matrix $\mathcal{M}$ by

$$ \langle\eta|\, \mathcal{M}\, |\overline{\eta}\rangle = \sum_{\eta'\overline{\eta}'} \langle\eta|\, \boldsymbol{\mathcal{E}}\cdot\mathbf{D}\, |\eta'\rangle\, \langle\eta'|\, \rho(0)\, |\overline{\eta}'\rangle\, \langle\overline{\eta}'|\, \boldsymbol{\mathcal{E}}\cdot\mathbf{D}\, |\overline{\eta}\rangle\,, \quad \text{(A.14)} $$

where $\boldsymbol{\mathcal{E}}$ is the polarization of the photoassociation light, that we will assume to be linear, $\mathbf{D}$ is the dipole operator, η (resp. η') is a $s+p$ (resp. $s+s$) state in the above coupling and $\rho(0)$ is the initial density matrix of the two atoms. The matrix $\mathcal{M}$ allows one to compute intensities in any intermediate coupling.

In the case of non-polarized atoms, the atoms are assumed to be in a $s+s$ state with given values F'_1 and F'_2, but with any value of $F'_{\rm t}$ and M'_F, and to have a relative motion with a small angular momentum ($\ell = 0$, 1, 2, 3 and 4). The initial state, $\rho(0)$, is thus assumed to be diagonal in the decoupled "atomic" basis, with equal weights for all considered two atom states and with unknown weights $f(\ell')$ for the different partial waves. In principle, for a given temperature, these weights are determined by the respective heights of the rotational barriers, but they can be changed by the presence of the so-called cooperative effects [28]. One has in any case

$$ \sum_{F_{\rm t},\ell'}(2F_{\rm t}+1)(2\ell'+1)f(\ell') = 1. \quad \text{(A.15)} $$

For linearly polarized light, equation (A.14) reads, apart from the vibrational overlap integral and from the

$$\langle 6s\ j_1\, I\, F_1\ 6p\ j_2\, I\, F_2\ F_{\rm t} M_F \epsilon; FM|\,\mathcal{M}\,|6s\ j_1\, I\, \overline{F}_1\ 6p\ \overline{j}_2\, I\, \overline{F}_2\ \overline{F}_{\rm t} \overline{M}_F \epsilon; FM\rangle = \delta_{F_{\rm t},\overline{F}_{\rm t}} \sum_{F'_{\rm t},\ell'\ (\epsilon=(-1)^{\ell'})} \frac{8}{3}\left(1+\epsilon(-1)^{F'_{\rm t}}\right) f(\ell')$$
$$\times \begin{pmatrix} F_{\rm t} & \ell' & F \\ M_F & 0 & -M_F \end{pmatrix} \begin{pmatrix} \overline{F}_{\rm t} & \ell' & F \\ \overline{M}_F & 0 & -\overline{M}_F \end{pmatrix} \mathcal{A}(j_2\,, F_1\,, F_2\,, F_{\rm t}, M_F, F'_1\,, F'_2\,, F'_{\rm t}) \mathcal{A}(\overline{j}_2\,, \overline{F}_1\,, \overline{F}_2\,, \overline{F}_{\rm t}, \overline{M}_F, F'_1\,, F'_2\,, \overline{F}'_{\rm t}), \quad \text{(A.16)}$$

$$\langle 6s\ j_1\, I\, F_1\ 6p\ j_2\, I\, F_2\ F_{\rm t} M_F \epsilon; FM|\,\mathcal{M}\,|6s\ j_1\, I\, \overline{F}_1\ 6p\ \overline{j}_2\, I\, \overline{F}_2\ \overline{F}_{\rm t} \overline{M}_F \epsilon; \overline{F}M\rangle =$$
$$8\,\delta_{F,F_{\rm t}}\,\delta_{\overline{F},\overline{F}_{\rm t}} \sum_{p=-1,0,1} \mathcal{B}(j_2\,, F_1\,, F_2\,, F_{\rm t}, M_F, F, F'_1\,, F'_2\,, F'_{\rm t}, p) \mathcal{B}(\overline{j}_2\,, \overline{F}_1\,, \overline{F}_2\,, \overline{F}_{\rm t}, \overline{F}, \overline{M}_F, F'_1\,, F'_2\,, F'_{\rm t}, p), \quad \text{(A.19)}$$

$$\mathcal{B}(j_2\,, F_1\,, F_2\,, F_{\rm t}, M_F, F'_1\,, F'_2\,, F'_{\rm t}, p) = (-1)^p \mathcal{E}_{-p} \begin{pmatrix} F & 1 & F'_{\rm t} \\ -M''_F - p & p & M''_F \end{pmatrix} \delta_{F_1\,,F'_1}\, \mathcal{S}(F_{\rm t}, M_F, 1, F)$$
$$\times (-1)^{3j_2+1/2F+F_{\rm t}+M_F}\, \widehat{j}_2\ \widehat{F}'_1 \widehat{F}_2\ \left[F'_{\rm t}\right] \widehat{F}/\widehat{1} \begin{pmatrix} F_{\rm t} & 0 & F \\ M_F & 0 & -M_F \end{pmatrix} \begin{Bmatrix} F_{\rm t} & 0 & F \\ F'_{\rm t} & 1 & F'_{\rm t} \end{Bmatrix} \begin{Bmatrix} F_{\rm t} & 1 & F'_{\rm t} \\ F'_2 & F'_1 & F_2 \end{Bmatrix} \begin{Bmatrix} F_2 & 1 & F'_2 \\ 1/2 & I & j_2 \end{Bmatrix}. \quad \text{(A.20)}$$

electronic orbital one,

see equation (A.16) above

with

$$\mathcal{A}(j_2\,, F_1\,, F_2\,, F_{\rm t}, M_F, F'_1\,, F'_2\,, F'_{\rm t}) =$$
$$\delta_{F_1\,,F'_1}\, \mathcal{S}(F_{\rm t}, M_F, \epsilon, F)\, (-1)^{3j_2+1/2+M_F}\, \widehat{j}_2\ \widehat{F}'_1 \widehat{F}_2\, \widehat{F}'_{\rm t}/\widehat{1}$$
$$\times \begin{pmatrix} F_{\rm t} & \ell' & F \\ M_F & 0 & -M_F \end{pmatrix} \begin{Bmatrix} F_{\rm t} & 1 & F'_{\rm t} \\ F'_2 & F'_1 & F_2 \end{Bmatrix} \begin{Bmatrix} F_2 & 1 & F'_2 \\ 1/2 & I & j_2 \end{Bmatrix} \quad \text{(A.17)}$$

and

$$\mathcal{S}(F_{\rm t}, M_F, \epsilon, F) = 1/\sqrt{2} \text{ if } M_F > 0$$
$$= 1/2 \text{ if } (M_F = 0 \text{ and } \epsilon = (-1)^{F_{\rm t}+F})$$
$$= 0 \text{ if } M_F < 0 \text{ or } (M_F = 0 \text{ and } \epsilon \neq (-1)^{F_{\rm t}+F}). \quad \text{(A.18)}$$

In the numerical results of Figure 9, the $f(\ell')$ are chosen to fit at best the experimental spectrum.

In the case of polarized atoms, the initial density matrix is restricted to a single Zeeman state f, m_f, so that one has $F'_1 = F'_2 = f$, $F'_{\rm t} = 2f$ and the projection of $F'_{\rm t}$ on the quantization axis is $M''_F = 2f$; one has also $\epsilon = 1$. In the experiment, it has been checked, on the 0^-_g spectrum, that the s-wave was providing the main contribution to the line intensities. Assuming thus $\ell' = 0$, we find

see equation (A.19) above

with

see equation (A.20) above.

The matrix $\mathcal{M}$ is not diagonal in F, but only the diagonal elements will be useful, because we are interested in eigenstates of $H_{\rm asympt} + B_v \boldsymbol{\ell}^2$, which commutes with $\mathbf{F}^2$.

References

1. J.T. Bahns, W.C. Stwalley, P.L. Gould, J. Chem. Phys. **104**, 9689 (1996).
2. A. Hermann, S. Leutwyler, L. Wöste, E. Schumacher, Chem. Phys. Lett. **62**, 444 (1979).
3. N. Djeu, W.T. Whitney, Phys. Rev. Lett. **46**, 236 (1981).
4. A. Kastler, J. Phys. Radium **11**, 255 (1950).
5. C.J. Bordé, N. Courtier, L. du Burck, A.N. Goncharov, M. Gorlicki, Phys. Lett. A **188**, 187 (1994).
6. U. Gaubatz, P. Rudecki, S. Schiemann, K. Bergmann, J. Chem. Phys. **92**, 5363 (1990).
7. P. Marte, P. Zoller, J.L. Hall, Phys. Rev. Lett. **44**, 4118 (1991).
8. P. Pillet, C. Valentin, R.L. Yuan, J. Yu, Phys. Rev. A **48**, 845 (1993).
9. L.S. Goldner, C. Gerz, R.J.C. Spreeuw, J.L. Rolston, C.I. Westbrook, W.D. Phillips, Phys. Rev. Lett. **72**, 997 (1994).
10. J. Lawall, M. Prentiss, Phys. Rev. Lett. **72**, 993 (1994).
11. M. Weitz, B.C. Young, S. Chu, Phys. Rev. Lett. **73**, 2563 (1994).
12. H.R. Thorsheim, J. Weiner, P.S. Julienne, Phys. Rev. Lett. **58**, 2420 (1987).
13. P.D. Lett, K. Helmerson, W.D. Phillips, L.P. Ratliff, S.L. Rolston, M.E. Wagshul, Phys. Rev. Lett. **71**, 2200 (1993).
14. J.D. Miller, R.A. Cline, D.J. Heinzen, Phys. Rev. Lett. **71**, 2204 (1993).
15. E.R.I. Abraham, N.W.M. Ritchie, W.I. McAlexander, R.G.Hulet, J. Chem. Phys. **103**, 7773 (1995);
16. H. Wang, P.L. Gould, W.C. Stwalley, Phys. Rev. A **53**, R1216 (1996).
17. A. Fioretti, D. Comparat, A. Crubellier, O. Dulieu, F. Masnou-Seeuws, P. Pillet, Phys. Rev. Lett. **80**, 4402 (1998).
18. A.P. Mosk, M.W. Reynolds, T.W. Hijmans, J.T.M. Walraven, Phys. Rev. Lett. **82**, 307 (1999).
19. R. Coté, A. Dalgarno, Chem. Rev. Lett. **279**, 50 (1997).

20. D. Comparat, C. Drag, A. Fioretti, O. Dulieu, P. Pillet, J. Mol. Spectrosc. **195**, 229 (1999).
21. Y.B. Band, P.S. Julienne, Phys. Rev. A **51**, R4317 (1995).
22. J.L. Bohn, P.S. Julienne, Phys. Rev. A **54**, R4637 (1996).
23. A.N. Nikolov, E.E. Eyler, X.T. Wang, J. Li, H. Wang, W.C. Stwalley, P.L. Gould, Phys. Rev. Lett. **82**, 703 (1999).
24. W. Ketterle, K.B. Davies, M.A. Joffe, A. Martin, D.E. Pritchard, Phys. Rev. Lett. **70**, 2253 (1993).
25. W.C. Stwalley, Y.H. Uang, G. Pichler, Phys. Rev. Lett. **41**, 1164 (1978).
26. X. Wang, H. Wang, P.L. Gould, W.C. Stwalley, E. Tiesinga, P. Julienne, Phys. Rev. A **57**, 4600 (1998).
27. A. Fioretti, D. Comparat, C. Drag, C. Amiot, O. Dulieu, F. Masnou-Seeuws, P. Pillet, Eur. Phys. J. D **5**, 389 (1999).
28. A. Fioretti, D. Comparat, C. Drag, T.F. Gallagher, P. Pillet, Phys. Rev. Lett. **82**, 1839 (1999).
29. C. Monroe, W. Swann, H. Robinson, C. Wieman, Phys. Rev. Lett. **65**, 1571 (1990).
30. S. Grego, M. Colla, A. Fioretti, J.H. Müller, P. Verkerk, E. Arimondo, Opt. Commun. **132**, 519 (1996).
31. C.G. Townsend, N.H. Edwards, K.P. Zetie, C.J. Cooper, J. Rink, C.J. Foot, Phys. Rev. A **53**, 1702 (1996).
32. I. Mourachko, Ph.D. thesis, University of Paris-Sud, 1999.
33. S. Gerstenkorn, J. Vergès, J. Chevillard, *Atlas du spectre d'absorption de la molécule d'iode* (laboratoire Aimé Cotton, Orsay, France, 1982).
34. G. Avila *et al.*, Metrologia **22**, 11 (1986).
35. E. Tiesinga, C.J. Williams, P.S. Julienne, K.M. Jones, P.D. Lett, W.D. Phillips, J. Res. Natl. Inst. Stand. Technol. **101**, 505 (1996).
36. M. Marinescu, H.R. Sadeghpour, A. Dalgarno, Phys. Rev. A **49**, 982 (1994)
37. M. Marinescu, A. Dalgarno, Phys. Rev. A **52**, 311 (1995)
38. G. Hadinger, G. Hadinger, S. Magnier, M. Aubert-Frecon, J. Mol. Spectrosc. **175**, 441 (1996).
39. U. Volz, H. Schmoranzer, Phys. Scripta T **65**, 48 (1996).
40. Bo Gao, Phys. Rev. A **54**, 2022 (1996).
41. C.C. Tsai, R.S. Freeland, J.M. Vogels, H.M.J.M. Boesten, B.J. Verhaar, D.J. Heinzen, Phys. Rev. Lett. **79**, 1245 (1997).
42. A. Lambrecht, E. Giacobino, S. Reynaud, Quant. Semiclass. **8**, 457 (1996).
43. D. Comparat, Ph.D. thesis, University of Paris-Sud, 1999.
44. P. Pillet, A. Crubellier, A. Bleton, O. Dulieu, P. Nosbaum, I. Mourachko, F. Masnou-Seeuws, J. Phys. B **30**, 2801 (1997).
45. J.M. Doyle, B. Friedrich, J. Kim, D. Patterson, Phys. Rev. A **52**, R2515 (1995).
46. J.D. Weinstein, R. de Carvalho, A. Martin, B. Friedrich, J.M. Doyle, Nature **395**, 148 (1998).
47. T. Takekoshi, B.M. Patterson, R.J. Knize, Phys. Rev. Lett. **81**, 5105 (1998).